ISSN 0915-633X

NATIONAL INSTITUTE FOR FUSION SCIENCE

Density-Carrying Particle Method for Fluid

S. Kawata, M. Shiromoto and T. Teramoto

(Received – Oct. 28, 1991)

NIFS-120 Nov. 1991

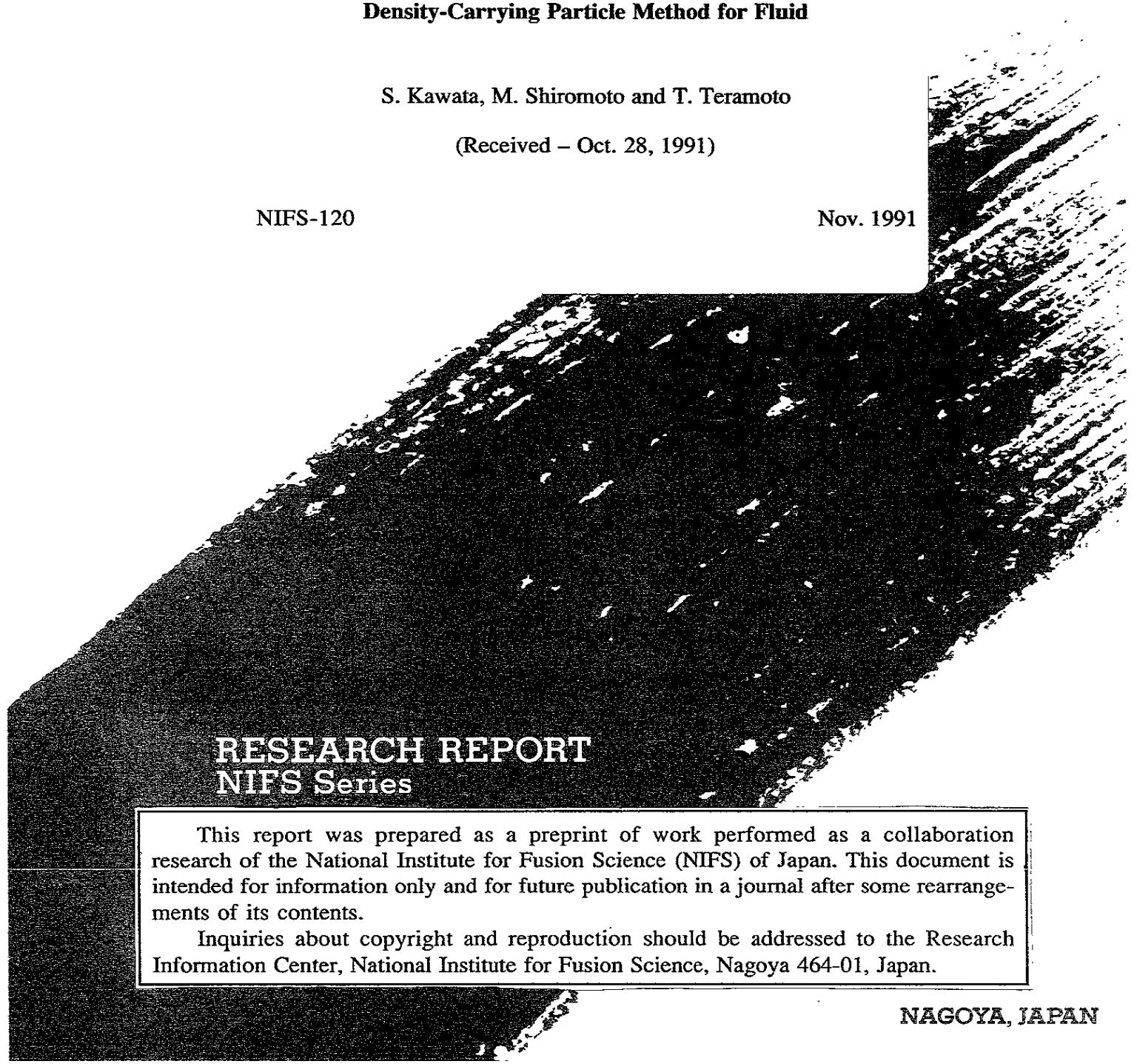

RESEARCH REPORT
NIFS Series

This report was prepared as a preprint of work performed as a collaboration research of the National Institute for Fusion Science (NIFS) of Japan. This document is intended for information only and for future publication in a journal after some rearrangements of its contents.

Inquiries about copyright and reproduction should be addressed to the Research Information Center, National Institute for Fusion Science, Nagoya 464-01, Japan.

NAGOYA, JAPAN

Density-Carrying Particle Method for Fluid

S. Kawata, M. Shiromoto AND T.Teramoto

Department of Electrical Engineering,
Nagaoka University of Technology,
Nagaoka 940-21,Japan

Abstract

A new particle method in which a numerical particle carries density of physical quantities, is introduced and discussed in this paper. In the conventional PIC method particles do not carry the density of physical quantities but carry the mass, momentum and energy themselves. In order to simulate the large change in the physical quantities, it is necessary to change the particle size. However the change in the particle size in the conventional PIC method may lead an unphysical error as shown in Fig.1, when it is applied inappropriately. Our particles carrying the density eliminate this unphysical error and can represent the large change in the physical quantities: One of example computations shows that in an adiabatic expansion the four figures of density change can be successfully simulated.

Key words: density-carrying particle method, particle-in-cell(PIC) method, fluid simulations, full-particle method, area-weighting method, compressible super particle

1. INTRODUCTION

A particle-in-cell(PIC) method has been presented by F.Harlow [1] for a computational scheme to analyze a meteoric impact problem. In this method, physical quantities such as a position, mass and energy, are carried by numerical "particles". The computation is proceeded by separating the fluid equations into two phases. In the first phase, the fluid equations without convection terms are solved on the grids. In the next phase, particles are pushed and the new values of physical quantities are computed by using the new particle position in order to include the convection effect. The PIC method has a great advantage to deal with a convection term in a simple way, so that it has been improved and applied to fluid simulations by many researchers [2-9]. Some of the methods have excellent advantages. Here, we introduce some of particle methods which are related to our work.

The full-particle method is presented by McCrory *et al.* [2], Leboeuf *et al.* [3] and so on. They attemped to assign more information to a particle for improving accurancy. They assign full information such as the position, mass, momentum, and energy onto a particle. In their method, a discontinuous pulse transpotation are accurately simulated, but difficulties with multistreaming and numerical noise are observed. The next one is presented by Nishiguchi and Yabe [4,5]. In their method, the mass and internal energy are carried by a particle, and in order to eliminate the first order diffusion the velocity is distributed inside the particle area. The particle has a compressibility in order to describe the large change of physical quantities.

In this paper we present a new particle method in which a compressible super particle carries the density of mass, momentum and energy. By using this density-carrying particle we can eliminate an unphysical error shown in Fig.1. This unphysical error may be introduced in the conventional PIC method with a compressible super particle, when it is applied inappropriately. In our method we can successfully simulate the large change of physical quantities without the unphysical error, as is shown in Fig.2. In the section 2 we present the motivation of our work. In the section 3 we describe the computational method for density-carrying particle method in detail. Then we demonstrate the viability

of our method in the section 4. The section 5 devotes to conclusions and discussions.

2. MOTIVATION

In the initial stage of PIC method development F.Harlow [1] presented his method in which the fluid was represented by Lagrangian mass points, moving through computational grids. The contribution to the change in each momentum and energy on the grids from the particle was considered when the particle moves across the grid boundary. This is so called the NGP(Nearest Grid Point) method. This method is the origin of the numerical noise. The area(or volume)-weighting method eliminates this noise successfully. One of disadvantages in the PIC method is that a large number of particles is required in order to describe the large change in the physical quantities. This was improved by Nishiguchi and Yabe [4,5]. They attemped to assign the compressibility to the particle. In their method, the particle volume is changed with the change of grid volume in order to simulate the large change in physical quantities. Their grid boundary can move with the arbitrary velocity. However this method may introduce an unphysical error which is demonstrated in Fig.1, when the method is applied inappropriately. Figure 1(a) shows the initial state, where the upper figure shows a particle being placed in grids. The particle has the same size as the cell size and stays at the center of cell which is denoted by circles. The lower figure shows the density profile, where a dotted line means the grid boundary. In Fig.1 the fluid is static with the flat profiles of density ρ and pressure, so that the density in each region has not to be changed. The density in the cell is determined by the following expression as is usual:

$$\rho_c = \frac{\sum_c m_p'}{V_c}, \tag{1}$$

where ρ_c, m_p' and V_c denote a mass density, a contributing part of a particle mass to the specified cell and a volume of cell, respectively. The summation is taken over particles contributing to the cell. When the mesh size is changed artifically as is shown in Fig.1(b), V_c is changed without any change in m_p' in eq(1) in Fig.1, and therefore the density is changed unexpectedly according to the grid motion in the conventional PIC method with a compressible particle. This is not acceptable in the computation.

In this paper we propose a new method to eliminate this unphysical error: In our method a compressible particle carries the density of mass, momentum and energy. For example, the mass density ρ_p in a cell is computed by

$$\rho_c = \frac{\sum_c W_p \rho_p}{\sum_c W_p}. \tag{2}$$

Here W_p is a particle weight contributing to the specified cell and ρ_p the particle mass density. Figure 2 shows our results for the same example presented in Fig.1. This example simulation demonstrates that our method describes the physical phenomena correctly, even when the particle size is changed with the artificial change in the mesh size; The density is not changed in time and is not changed by the change of particle size. We describe the detail of our method in the following section.

3. COMPUTATIONAL METHOD FOR DENSITY- CARRYING PARTICLE METHOD

a. Compressible Fluid Equations

In this section we present the detail about the computational method of the density-carrying particle method. As it is well known, the equation of continuous, momentum and energy is represented as follows:

$$\frac{\partial \rho}{\partial t} + \vec{\nabla} \cdot (\rho \vec{v}) = 0, \tag{3}$$

$$\frac{\partial \rho \vec{v}}{\partial t} + \vec{\nabla} \rho \vec{v} \vec{v} = -\vec{\nabla} P, \tag{4}$$

$$\frac{\partial \rho e}{\partial t} + \vec{\nabla} \cdot \rho \vec{v} e = -P \vec{\nabla} \cdot \vec{v}, \tag{5}$$

where $\rho, \vec{v}, P$, and e denote the mass density, velocity, pressure and specific internal energy. First, we transform the three equations as follows:

$$\frac{\partial \rho}{\partial t} + \vec{v} \vec{\nabla} \rho + \rho \vec{\nabla} \cdot \vec{v} = 0, \tag{6}$$

$$\frac{\partial \vec{v}}{\partial t} + \vec{v}\vec{\nabla}\vec{v} = -\frac{1}{\rho}\vec{\nabla}P, \tag{7}$$

$$\frac{\partial \rho e}{\partial t} + \vec{v}\cdot\vec{\nabla}\rho e + \rho e\vec{\nabla}\cdot\vec{v} = -P\vec{\nabla}\cdot\vec{v}, \tag{8}$$

where the second term of the left hand side in each equation shows the convection term. In PIC method, this term is represented by the particle movement through the cell.

b. Euler phase

As the basic equations for the Euler phase, we drop each convection term in eqs.(6),(7) and (8):

$$\frac{\partial \rho}{\partial t} = -\rho\vec{\nabla}\cdot\vec{v}, \tag{9}$$

$$\frac{\partial \vec{v}}{\partial t} = -\frac{1}{\rho}\vec{\nabla}P, \tag{10}$$

$$\frac{\partial E}{\partial t} = -(P+E)\vec{\nabla}\cdot\vec{v}, \tag{11}$$

where E is used instead of ρe and denoted the internal-energy density. For simplicity, we consider the one-dimensional fluid equations:

$$\frac{\partial \rho}{\partial t} = -\rho\frac{\partial u}{\partial x}, \tag{12}$$

$$\frac{\partial u}{\partial t} = -\frac{1}{\rho}\frac{\partial P}{\partial x}, \tag{13}$$

$$\frac{\partial E}{\partial t} = -(P+E)\frac{\partial u}{\partial x}, \tag{14}$$

In the finite difference form, three equations become:

$$\widetilde{\delta\rho_{c,i}} = -\rho^{n*}_{c,i}\Delta t\frac{u^{n*}_{c,i+1/2} - u^{n*}_{c,i-1/2}}{\Delta x}, \tag{15}$$

$$\widetilde{\delta u_{c,i-1/2}} = -\frac{\Delta t}{\rho^{n*}_{c,i}}\frac{P^{n*}_{c,i} - P^{n*}_{c,i-1}}{\Delta x}, \tag{16}$$

$$\widetilde{\delta E_{c,i}} = -(P^{n*}_{c,i} + E^{n*}_{c,i})\Delta t\left(\frac{u^{n*}_{c,i+1/2} - u^{n*}_{c,i-1/2}}{\Delta x}\right). \tag{17}$$

Figure 3 shows the space-mesh structure. The superscript shows the index for time and $n* = n + 1/2$. The physical quantity attached with the subscript c means its value

computed on the grid or the cell center. The mass density, pressure and internal-energy density are defined at the cell center and the others are at the grid point. The physical quantity with ~ indicates the tentative value. By attaching δ, the increment in physical quantities during the timestep Δt is represented. Therefore the tentative values are obtained as follows:

$$\widetilde{\rho_{c,i}} = \rho^n_{c,i} + \widetilde{\delta\rho_{c,i}}, \tag{18}$$

$$\widetilde{u_{c,i-1/2}} = u^n_{c,i-1/2} + \widetilde{\delta u_{c,i-1/2}}, \tag{19}$$

$$\widetilde{E_{c,i}} = E^n_{c,i} + \widetilde{\delta E_{c,i}}, \tag{20}$$

$$\Psi^{n*} = \frac{\Psi^n + \tilde{\Psi}}{2}. \tag{21}$$

Here Ψ means the physical quantities representatively. In the Euler phase eqs.(15)-(21) are solved implicitly and iteratively.

c. Particle-mesh interaction and particle push

In this subsection, we describe the particle-mesh interaction and particle push algorithm. The increment in each physical quantity of a particle is determined by the area-weighting method from the eqs.(15)-(17). This one-dimensional interpolation is decribed schematically in Fig.4. Figure 4(a) shows the present state and Fig.4.(b) the later state. The area are A_i and B_i which are obtained by the overlapped region between a particle cloud and cell. The particle has the same size as the size of the smaller cell of two adjacent cells overlapping the particle. Then we obtain the increment in the particle quantities:

$$\delta\rho_p = A_1\widetilde{\delta\rho_{c,i}} + A_2\widetilde{\delta\rho_{c,i+1}}, \tag{22}$$

$$\delta u_p = A'_1\widetilde{\delta u_{c,i-1/2}} + A'_2\widetilde{\delta u_{c,i+1/2}}, \tag{23}$$

$$\delta E_p = A_1\widetilde{\delta E_{c,i}} + A_2\widetilde{\delta E_{c,i+1}}, \tag{24}$$

where the quantity with the subscript p shows the particle one. The area A_j and A'_j mean the weights. Then we obtain new quantities of particle from eqs.(22),(23) and (24):

$$\rho^{n+1}_p = \rho^n_p + \delta\rho_p, \tag{25}$$

$$(\rho_p u_p)^{n+1} = (\rho_p u_p)^n + (\delta\rho_p)u_p^n + \rho_p^n(\delta u_p), \tag{26}$$

$$E_p^{n+1} = E_p^n + \delta E_p. \tag{27}$$

Next the particle is pushed by the velocity u_{convec}:

$$u_{convec} = A_1^{'}\widetilde{u}_{c,i-1/2} + A_2^{'}\widetilde{u}_{c,i+1/2}, \tag{28}$$

where u_{convec} is determined by the interpolation from the cell velocity $\widetilde{u_c}$. We employ this treatment in order to include a collisional fluid property and to avoid the multistreaming. This prescription is the same as that given by Brackbill [7]. From eq.(28) we obtain the new position of the particle:

$$x_p^{n+1} = x_p^n + u_{convec}\Delta t. \tag{29}$$

Finally, we compute the contribution from the particle to the cell. By the area-weighting method as shown in Fig.4(b), we present the contribution of one particle to a cell:

$$U_i^{n+1} = B_1 U_p^{n+1}, \tag{30}$$

$$U_{i+1}^{n+1} = B_2 U_p^{n+1}. \tag{31}$$

The physical quantities are obtained by the following expressions:

$$\rho_{c,i}^{n+1} = \frac{\sum\limits_p B_p \rho_p^{n+1}}{\sum\limits_p B_p}, \tag{32}$$

$$u_{c,i-1/2}^{n+1} = \frac{\sum\limits_p B_p^{'} u_p^{n+1}}{\sum\limits_p B_p^{'}}, \tag{33}$$

$$E_{c,i}^{n+1} = \frac{\sum\limits_p B_p E_p^{n+1}}{\sum\limits_p B_p}. \tag{34}$$

In these eqs.(30)-(34) B_p and $B_{p'}$ show the contribution weights of the particle to the cell and the summation is taken over the particles contributing to the specified cell.

d. Computation Cycle

In this subsection, we review the computation cycle. The flow chart is described in Fig.5. We present the sequence of computational flow. The following number corresponds to the number in the flow chart.

(1) We compute the increment in the physical quantities on a cell by eqs.(15)-(17):

$$\widetilde{\delta\rho_{c,i}} = -\rho^{n*}_{c,i}\Delta t\frac{u^{n*}_{c,i+1/2} - u^{n*}_{c,i-1/2}}{\Delta x}, \tag{15}$$

$$\widetilde{\delta u_{c,i-1/2}} = -\frac{\Delta t}{\rho^{n*}_{c,i}}\frac{P^{n*}_{c,i} - P^{n*}_{c,i-1}}{\Delta x}, \tag{16}$$

$$\widetilde{\delta E_{c,i}} = -(P^{n*}_{c,i} + E^{n*}_{c,i})\Delta t(\frac{u^{n*}_{c,i+1/2} - u^{n*}_{c,i-1/2}}{\Delta x}). \tag{17}$$

(2) We obtain the increment in the physical quantities on a particle from a cell by the area-weighting interpolation:

$$\delta\rho_p = A_1\widetilde{\delta\rho_{c,i}} + A_2\widetilde{\delta\rho_{c,i+1}}, \tag{22}$$

$$\delta u_p = A'_1\widetilde{\delta u_{c,i-1/2}} + A'_2\widetilde{\delta u_{c,i+1/2}}, \tag{23}$$

$$\delta E_p = A_1\widetilde{\delta E_{c,i}} + A_2\widetilde{\delta E_{c,i+1}}. \tag{24}$$

The exressions for the physical quantities themselves are eqs.(25)-(27).

$$\rho_p^{n+1} = \rho_p^n + \delta\rho_p, \tag{25}$$

$$(\rho_p u_p)^{n+1} = (\rho_p u_p)^n + (\delta\rho_p)u_p^n + \rho_p^n(\delta u_p), \tag{26}$$

$$E_p^{n+1} = E_p^n + \delta E_p. \tag{27}$$

(3) The particle is pushed to the new position by the velocity of eq.(28)

$$x_p^{n+1} = x_p^n + u_{convec}\Delta t. \qquad (29)$$

(4) The new grid position is computed by an appropriate velocity $u_{g,i}$ which can be selected arbitrary;

$$x_{c,i}^{n+1} = x_{c,i}^n + u_{g,i}\Delta t, \qquad (35)$$

For example, when $u_{g,i} = 0$, the scheme is the Euler one, and when $u_{g,i} = u_{c,i}$, it is the Lagrange one.

(5) We compute the cell quantities based on the new particle position, the new grid position and the new particle quantities by the area-weighting interpolation:

$$\rho_{c,i}^{n+1} = \frac{\sum_p B_p \rho_p^{n+1}}{\sum_p B_p}, \qquad (36)$$

$$(\rho_c u_c)_i^{n+1} = \frac{\sum_p B_p' (\rho_p u_p)^{n+1}}{\sum_p B_p'}, \qquad (37)$$

$$E_{c,i}^{n+1} = \frac{\sum_p B_p E_p^{n+1}}{\sum_p B_p}, \qquad (38)$$

$$u_{c,i}^{n+1} = \frac{(\rho_c u_c)_i^{n+1}}{\rho_{c,i}^{n+1}}. \qquad (39)$$

where $\sum_p$ means the summation over all particles contributing to the specified cell. Since we obtain full information of cell and particle which are necessary to update the computation, we return to the first step.

4. Numerical Results and Conservation Laws

In this section, let us introduce some simulation results by the density-carrying particle method. First, we present a simulation for square-pulse propagation. Figure 6(a) and (b) are the first state of a square-pulse and the state of 200 time-step later, respectively. This simulation is performed by solving the continuous equation at a constant velocity. As is well known, full-particle method is powerful to describe such a discontinuous surface. From the results of Fig.6 our method has also this advantage.

Next, we applied our method to a shock tube simulation. Figure 7 shows the profiles of the pressure, velocity and density, respectively. The solid line shows the analytical results and the squares show the simulational results. In our method, an artificial viscosity is used in the combinational form:

$$q = q_1 + q_2, \tag{40}$$

where

$$q_1 = \begin{cases} -a_1 \rho C_s (\frac{\partial u}{\partial x})(\Delta x), & \text{if } \frac{\partial u}{\partial x} < 0; \\ 0, & \text{otherwise.} \end{cases} \tag{41}$$

$$q_2 = \begin{cases} a_2 \rho (\frac{\partial u}{\partial x})^2 (\Delta x)^2, & \text{if } \frac{\partial u}{\partial x} < 0; \\ 0, & \text{otherwise.} \end{cases} \tag{42}$$

Here C_s means the sound speed, and a_1 and a_2 are adjustable constants of order unity. Figure 7 shows that the shock-tube problem is also simulated successfuly by our method. The pressure of the lower region is setted to $P = 1.0$ and the higher one is $P = 10.0$. We employed 80 space grids and 4 particles per one mesh at the initial time for this simulation. The cell boundaries moved with the velocity of $u_{g,i} = \frac{u_{c,i-1} + u_{c,i} + u_{c,i+1}}{3}$. We also checked the conservation laws for this shock-tube simulation. In order to check the conservation laws we employed the following formulations:

$$\Delta\rho = \frac{\sum_i \rho_{c,i} \Delta V_i - M_{t,0}}{M_{t,0}}, \tag{43}$$

$$\Delta E = \frac{\sum_i (E_{c,i} + \frac{1}{2}\rho_{c,i} u_{c,i}^2)\Delta V_i - E_{t,0}}{E_{t,0}}, \tag{44}$$

where

$$\Delta V_i = x_{c,i+1/2} - x_{c,i-1/2}, \tag{45}$$

$$u_{c,i} = \frac{1}{2}(u_{c,i-1/2} + u_{c,i+1/2}). \tag{46}$$

Here, $M_{t,0}$ and $E_{t,0}$ are the initial total mass and energy, respectively. This computation results for the conservation law check are shown in Fig.8.(a)-(b). In this case the mass-conservation error was less than 0.2% and the energy-conservation error was kept to be less than 0.5% during the whole computation. Our method keeps the conservation laws correctly.

In order to demonstrate a viability of our method for the simulation of the large change in the physical quantity, we performed the one-dimensional adiabatic-expansion simulation. In this case both boundaries of a cell move with a fixed speed to the opposite directions with each other to expand the fluid in cell. We employ three particles per cell initially. The pressure and density of an ideal fluid should obey the adiabatic law as shown by the solid line in Fig.9. The simulation result is denoted by squares. We simulate successfully the four figures of density change in our method.

5. Conclusions and Discussions

In the conventional particle method a particle had no compressibility so that it was difficult to deal with the comprehensive change in the physical quantity. In order to solve this advantage, previous researchers [4-5] have attempted to assign the comperssibility to the particle. By this improvement we were able to simulate the large change in the physical quantities. However we found that such the improvement might introduce unphysical error shown in Fig.1 when it is applied inappropriately. In this paper we presented a new method which does not introduce unphysical error. By employing this method we simulated successfuly a square-pulse propagation, a shock-tube problem and an adiabatic expansion. These results demonstrated the following features of our method.

(1) Our particle method carrys the density of physical quantities and the unphysical error was removed.

(2) Our method has also the ability to simulate a discontinuous step correctly as well as the conventional full-particle method.

(3) The large change in the physical quantities can be simulated by the grid movement and the compressibility of the particle.

Though we employ the low-order area-weighting method in this paper, the higher-order one, for example, by Nishiguchi and Yabe[4-5] can be also applied. The extension to the multi-dimensional version can be also easily attained.

Acknowledgements

This work is partly supported by the Scientific Research Fund of the Ministry of Education and Culture in Japan, and also in part supported by the cooperation program in the National Institute for Fusion Science in Japan.

References

1) F.H.Harlow : Meth. Comput. Phys. **3**, 319 (1963),

2) R.L.McCrory, R.L.Morse, and K.A.Taggart : Nucl. Sci. Eng. **64**, 163 (1977),

3) J.N.Leboeuf, T.Tajima, and J.M.Dawson : J. Comput. Phys. **31**, 379 (1979),

4) Nishiguchi and Yabe : J. Comput. Phys. **47**, 297 (1982),

5) Nishiguchi and Yabe : J. Comput. Phys. **52**, 390 (1983),

6) J.J.Monaghan : Comput. Phys. Rep. **3**,71 (1985),

7) J.U.Brackbill and H.M.Ruppel : J. Comput. Phys. **65**,314 (1986),

8) J.U.Brackbill : Comput. Phys. Communi. bf47,1 (1987),

9) J.U.Brackbill : J. Comput. Phys. **96**, 163 (1991),

10) H.Takewaki and T.Yabe : J. Comput. Phys. **61**, 261 (1985),

11) H.Takewaki and T.Yabe : J. Comput. Phys. **61**, 519 (1985),

12) R.W.Hockney and J.W.Eastwood, *Computer Simulation Using Particle* (McGraw-Hill, New York, 1981),

13) edited by J.U.Brackbill and J.J.Monaghan, *Proc. of the Workshop on Particle*

Method in Fluid Dynamics and Plasma Physics (North-Holland, Amsterdam, 1988),
14) T.Tajima, *Computational Plasma Physics: With Applications to Fusion and Astrophysics* (Addison-Wesley, New York, 1989),

Figure captions

Fig.1.(a) Initial state of static fluid simulation by a conventional method with a compressible particle whose size is changed with the change of cell size in order to describe the large change in physical quantities. The upper figure denotes the positions of cell and the particle. The particle stays at the center of each circles. The dotted lines show the cell boundaries. In the initial state the particle has the same size as the cell size. The lower figure is the density profile of the cell. (b) Later state of the static fluid simulation by the conventional method. The dash-dotted lines denote the initial cell boundaries. According to the change of the cell volume, the density of the cell is unexpectedly changed(see eq.(1)).

Fig.2.(a) Initial state of static fluid simulation by a density-carrying particle method. The initial state is the same as Fig.1(a). (b) Later state of the static fluid simulation by our method. The dash-dotted lines denote the initial cell boundaries. Even though the volume of each cell is changed by the movement of cell boundary, the density profile is not changed successfully(see eq.(2)).

Fig.3 One-dimensional space-mesh structure. The mass, pressure and internal energy are defined at the position at $\times$ and the velocity is defined at the cell boundary.

Fig.4 One-dimensional area-weighting method for the present method. (a) A state before the particle push and (b) after the particle push.

Fig.5 Flow chart for the Density-Carrying Particle Method.

Fig.6 Square-pulse propagation at first state. (a) Initial state and (b) the state of 200-time-step later.

Fig.7 Shock-tube simulation. The solid lines and squares denote analytical and simulation results, respectively. The cell boundaries moved with the velocity $u_{g,i} = \frac{u_{c,i-1} + u_{c,i} + u_{c,i+1}}{3}$.

Fig.8.(a) Time sequence of mass-conservation error and (b) of energy-conservation error.

Fig.9 Adiabatic expansion simulation. The solid line and squares denote theoritical and simulation results, respectively. We employed three particles per cell.

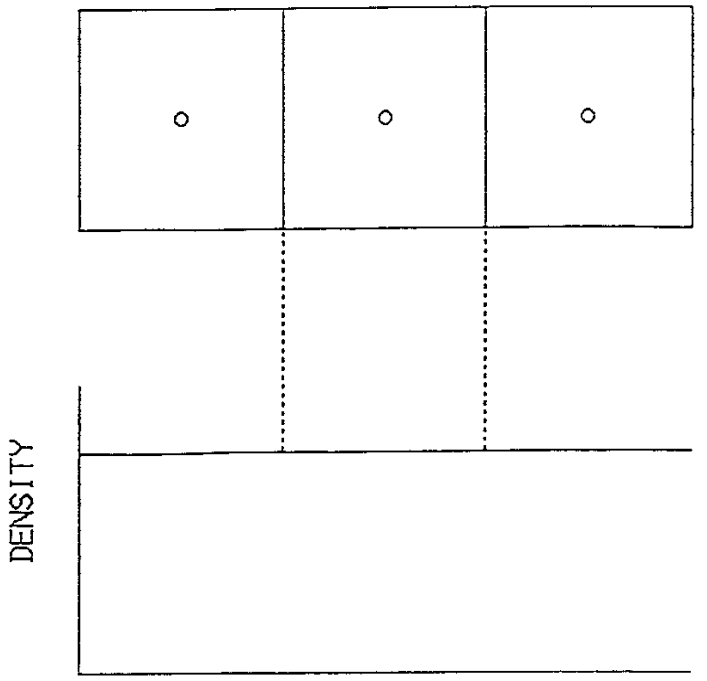

(a) Initial State(conventional method)

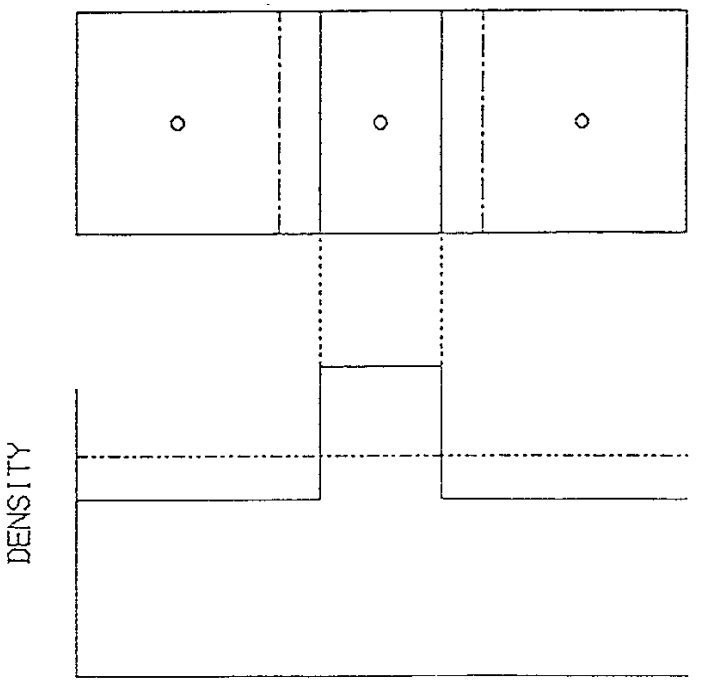

(b) Later State(conventional method)

Fig.1

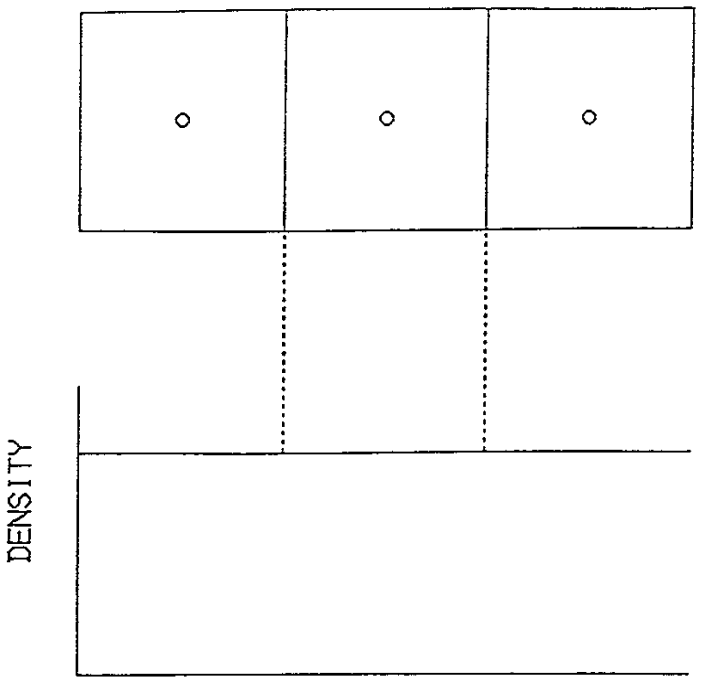

(a) Initial State(our method)

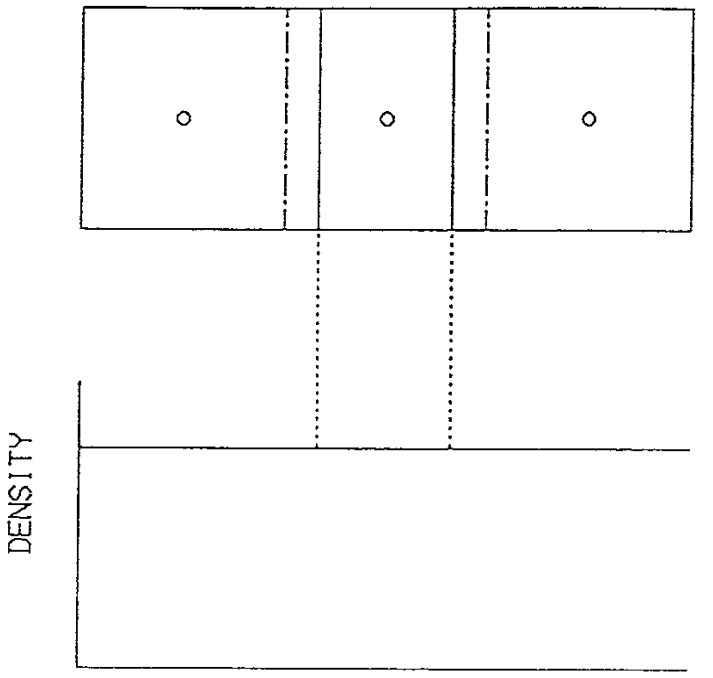

(b) Later State(our method)

Fig.2

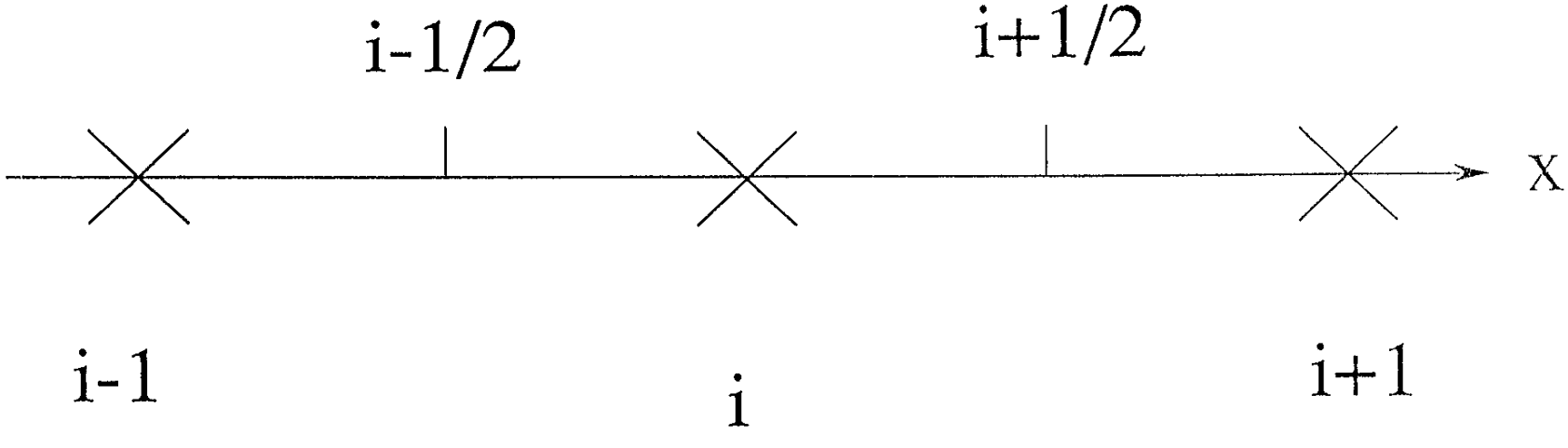

Fig.3

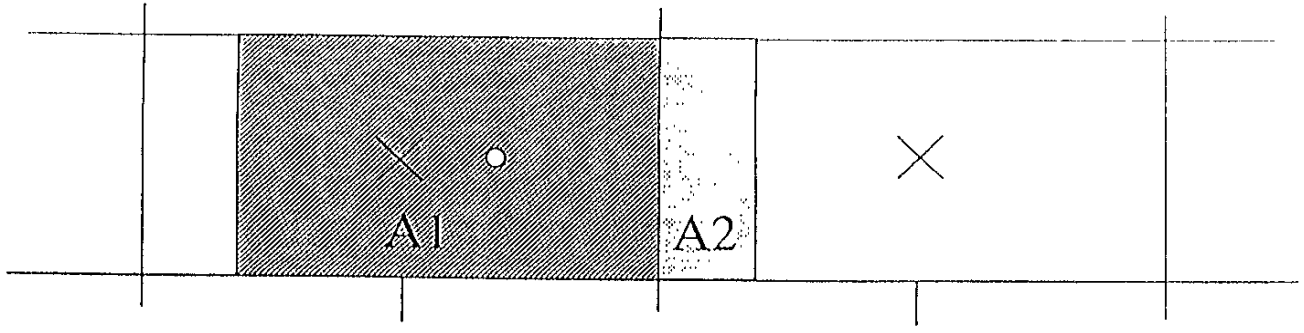

(a)

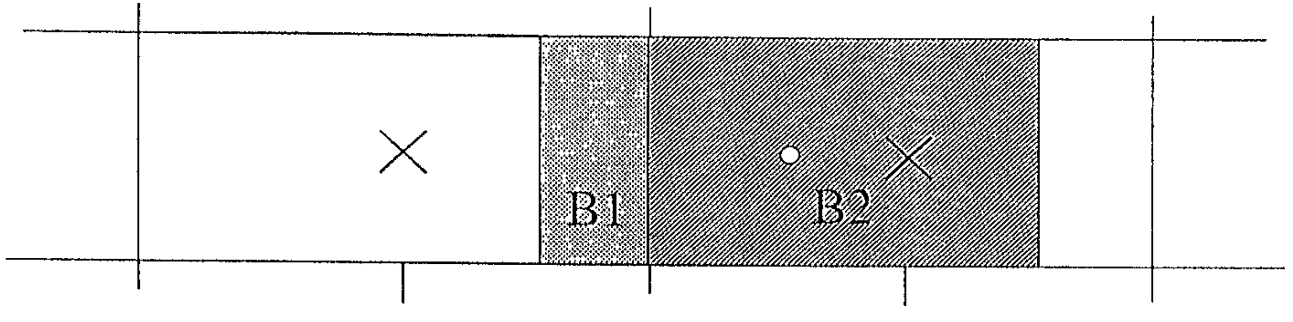

(b)

Fig.4

FLOW CHART

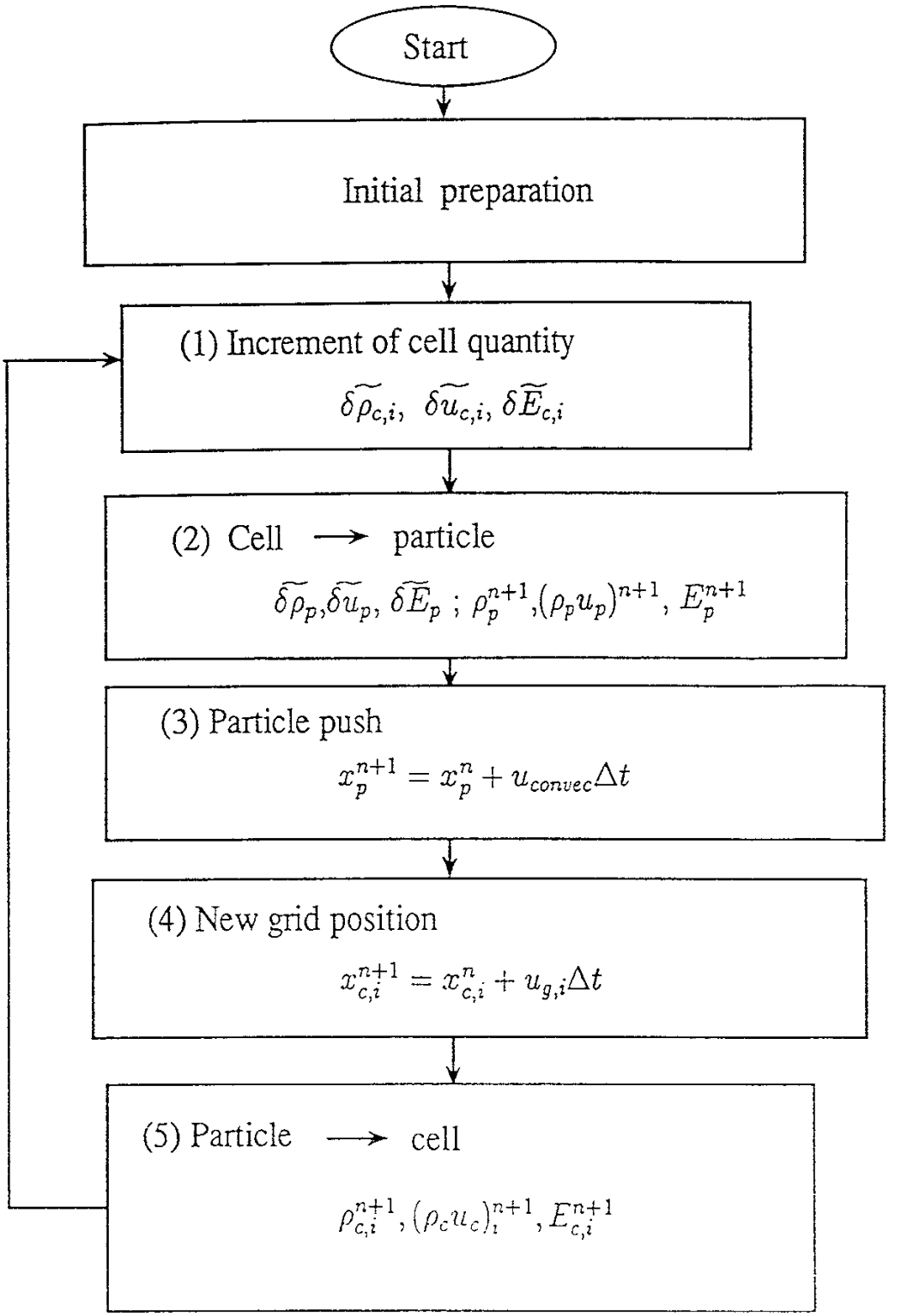

Fig.5

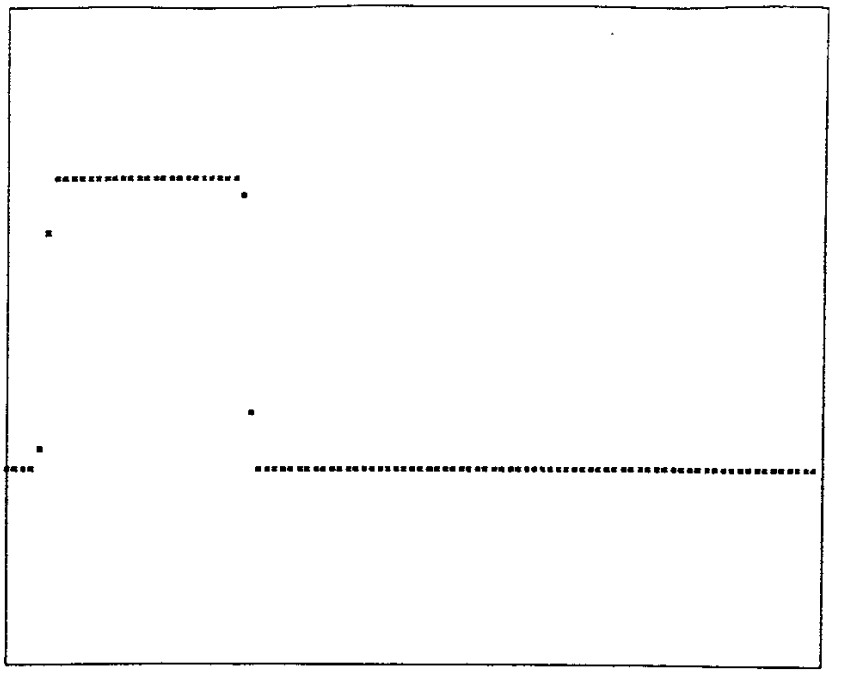

(a)

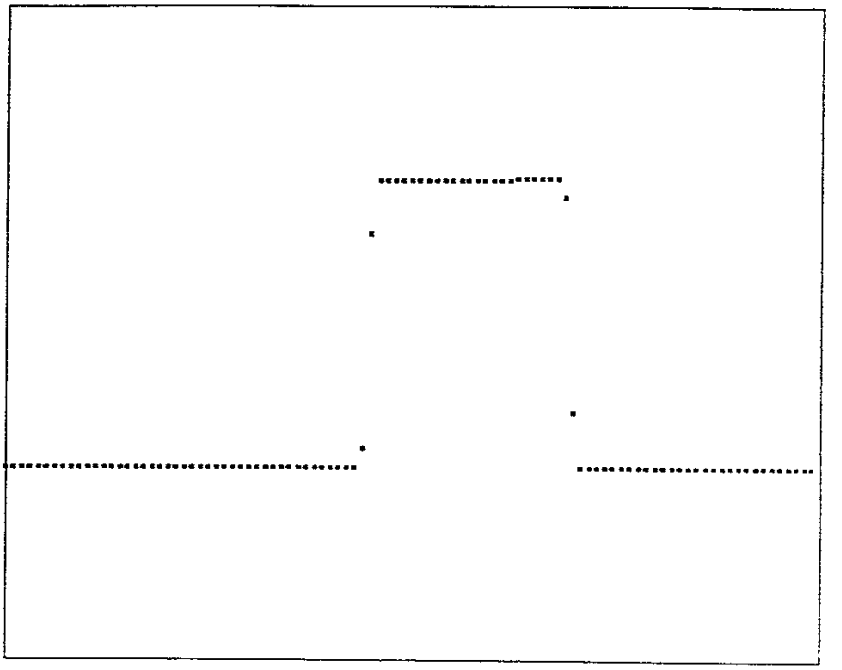

(b)

Fig.6

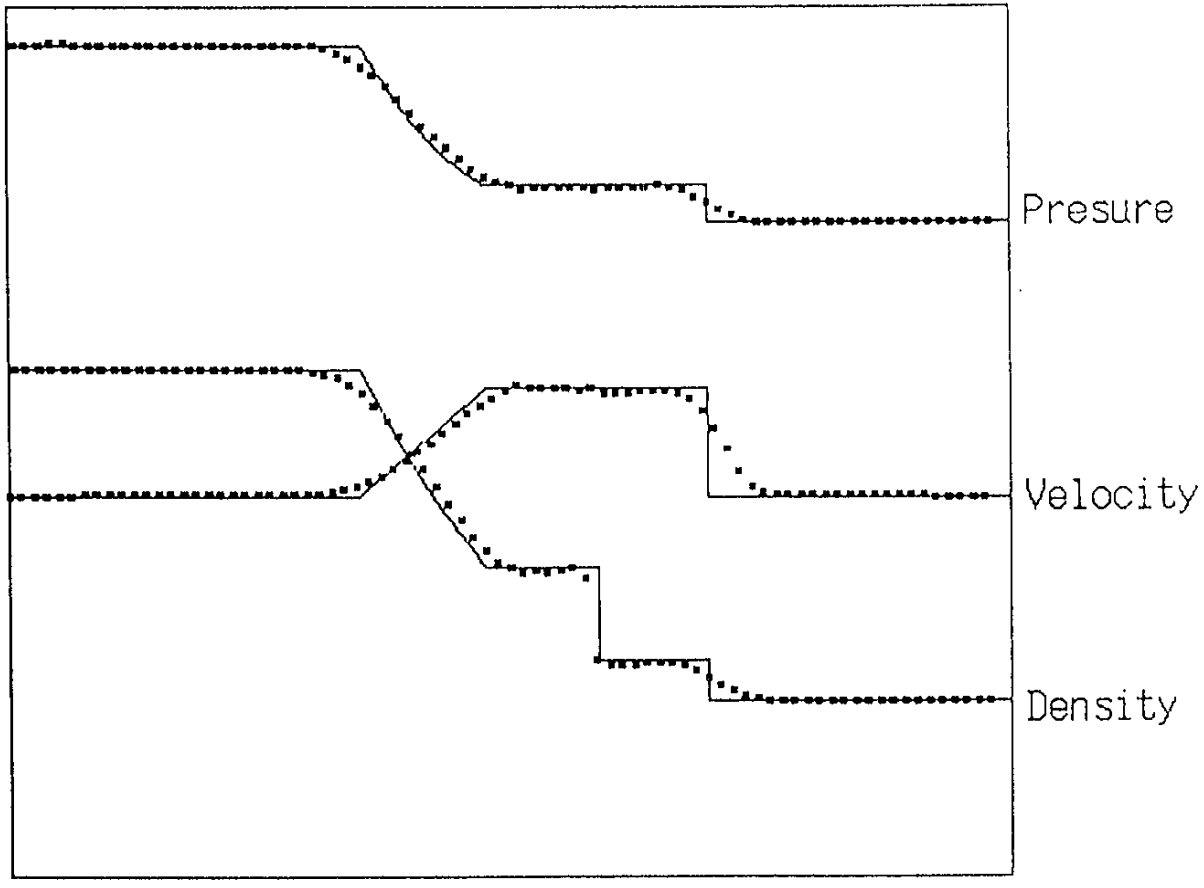

Fig.7

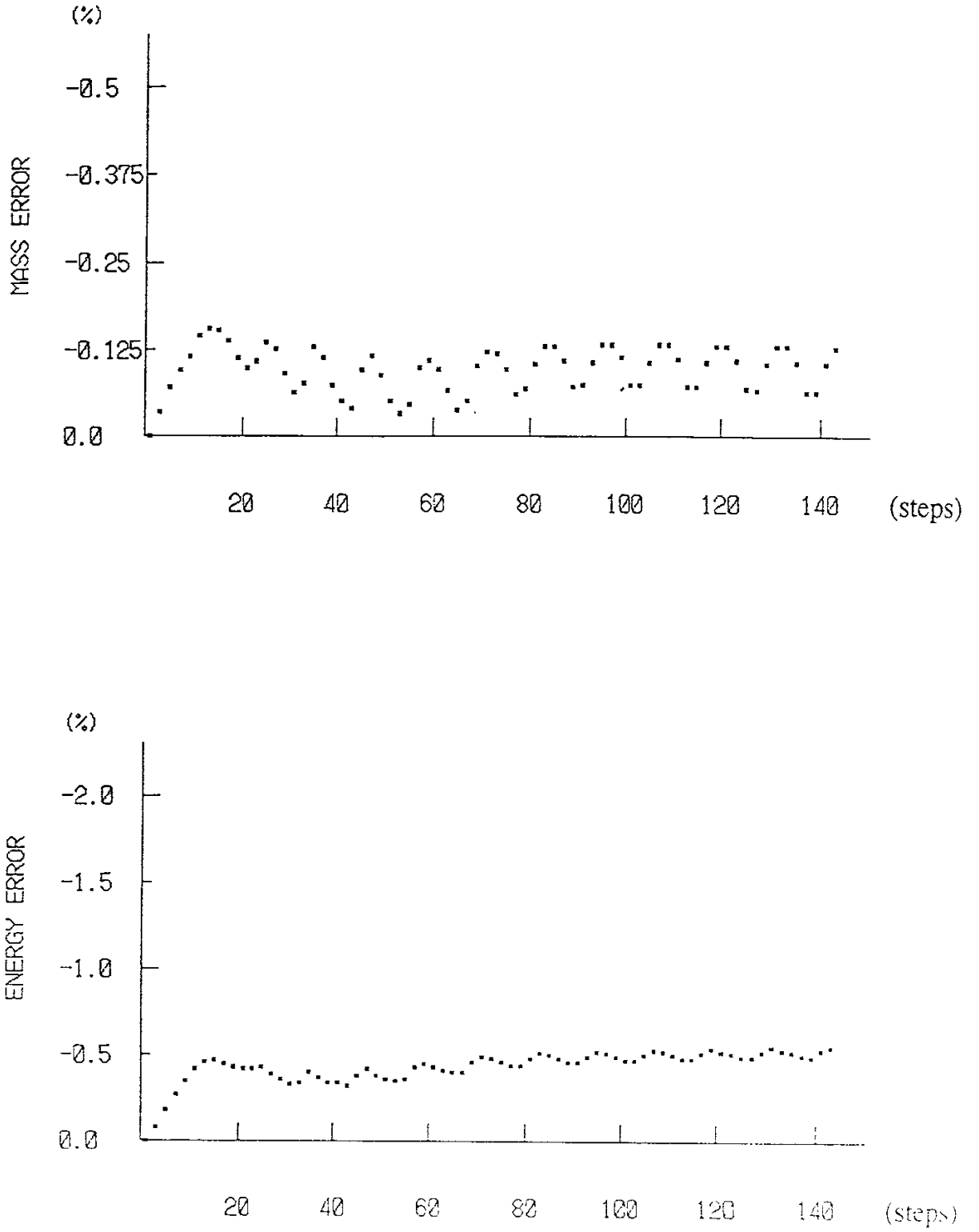
(%)
-0.5
-0.375
-0.25
-0.125
0.0
MASS ERROR
20
40
60
80
100
120
140
(steps)
(%)
-2.0
-1.5
-1.0
-0.5
0.0
ENERGY ERROR
20
40
60
80
100
120
140
(steps)

Fig.8

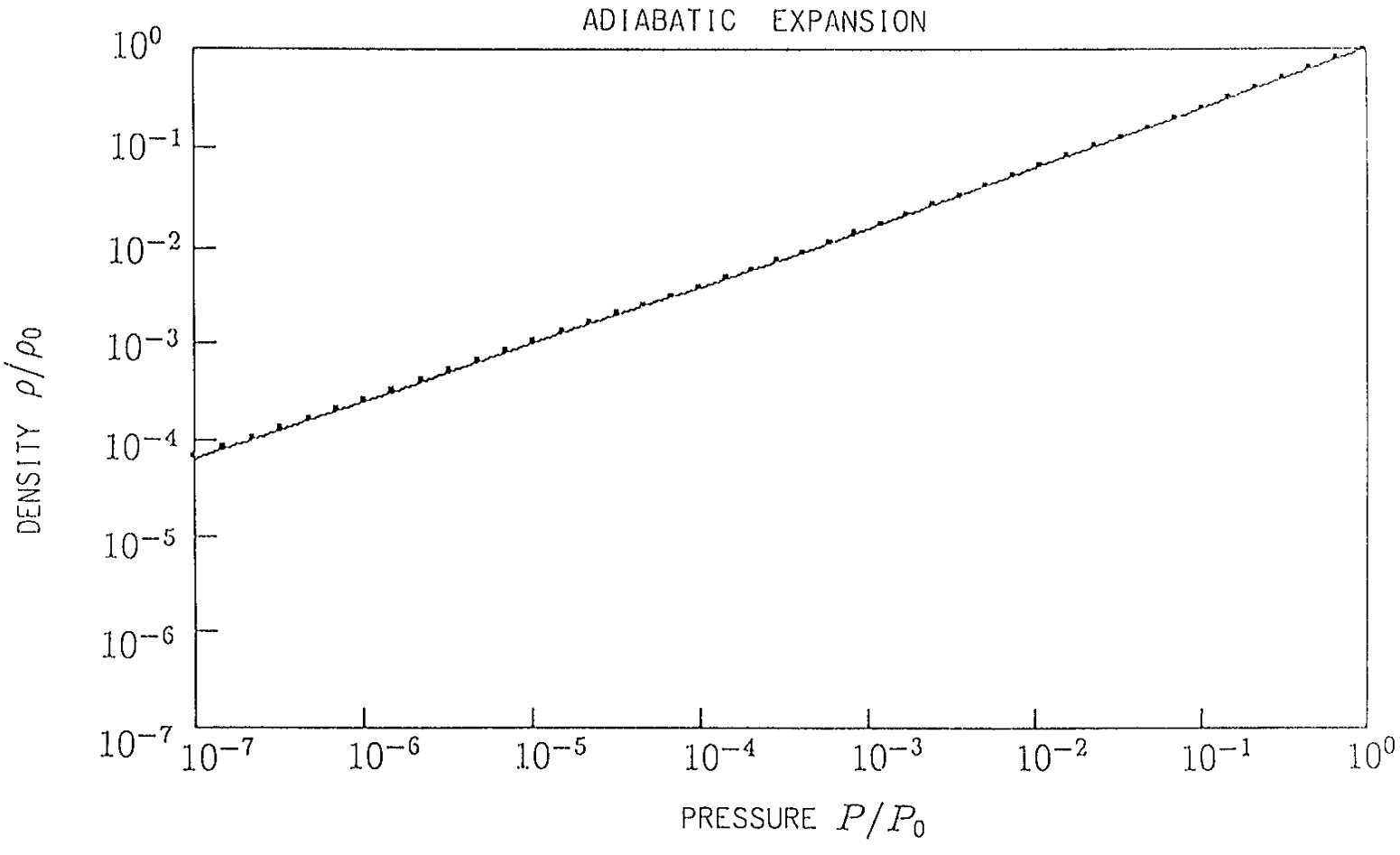
ADIABATIC EXPANSION
DENSITY ρ/ρ_0
10^0
10^{-1}
10^{-2}
10^{-3}
10^{-4}
10^{-5}
10^{-6}
10^{-7}
10^{-7}
10^{-6}
10^{-5}
10^{-4}
10^{-3}
10^{-2}
10^{-1}
10^0
PRESSURE P/P_0

Fig.9

Recent Issues of NIFS Series

NIFS-60 K.Ida, H.Yamada, H.Iguchi, S.Hidekuma, H.Sanuki, K.Yamazaki and CHS Group, *Electric Field Profile of CHS Heliotron/Torsatron Plasma with Tangential Neutral Beam Injection*; Oct. 1990

NIFS-61 T.Yabe and H.Hoshino, *Two- and Three-Dimensional Behavior of Rayleigh-Taylor and Kelvin-Helmholz Instabilities*; Oct. 1990

NIFS-62 H.B. Stewart, *Application of Fixed Point Theory to Chaotic Attractors of Forced Oscillators;* Nov. 1990

NIFS-63 K.Konn., M.Mituhashi, Yoshi H.Ichikawa,*Soliton on Thin Vortex Filament;* Dec. 1990

NIFS-64 K.Itoh, S.-I.Itoh and A.Fukuyama,*Impact of Improved Confinement on Fusion Research;* Dec. 1990

NIFS -65 A.Fukuyama, S.-I.Itoh and K. Itoh,*A Consistency Analysis on the Tokamak Reactor Plasmas;* Dec. 1990

NIFS-66 K.Itoh, H. Sanuki, S.-I. Itoh and K. Tani,*Effect of Radial Electric Field on α-Particle Loss in Tokamaks;* Dec. 1990

NIFS-67 K.Sato,and F.Miyawaki,*Effects of a Nonuniform Open Magnetic Field on the Plasma Presheath*; Jan.1991

NIFS-68 K.Itoh and S.-I.Itoh,*On Relation between Local Transport Coefficient and Global Confinement Scaling Law;* Jan. 1991

NIFS-69 T.Kato, K.Masai, T.Fujimoto,F.Koike, E.Källne, E.S.Marmar and J.E.Rice,*He-like Spectra Through Charge Exchange Processes in Tokamak Plasmas;* Jan.1991

NIFS-70 K. Ida, H. Yamada, H. Iguchi, K. Itoh and CHS Group, *Observation of Parallel Viscosity in the CHS Heliotron/Torsatron* ; Jan.1991

NIFS-71 H. Kaneko, *Spectral Analysis of the Heliotron Field with the Toroidal Harmonic Function in a Study of the Structure of Built-in Divertor* ; Jan. 1991

NIFS-72 S. -I. Itoh, H. Sanuki and K. Itoh, *Effect of Electric Field Inhomogeneities on Drift Wave Instabilities and Anomalous Transport* ; Jan. 1991

NIFS-73 Y.Nomura, Yoshi.H.Ichikawa and W.Horton, *Stabilities of Regular Motion in the Relativistic Standard Map*; Feb. 1991

NIFS-74 T.Yamagishi, *Electrostatic Drift Mode in Toroidal Plasma with Minority Energetic Particles*, Feb. 1991

NIFS-75 T.Yamagishi, *Effect of Energetic Particle Distribution on Bounce Resonance Excitation of the Ideal Ballooning Mode*, Feb. 1991

NIFS-76 T.Hayashi, A.Tadei, N.Ohyabu and T.Sato, *Suppression of Magnetic Surface Breading by Simple Extra Coils in Finite Beta Equilibrium of Helical System;* Feb. 1991

NIFS-77 N. Ohyabu, *High Temperature Divertor Plasma Operation*; Feb. 1991

NIFS-78 K.Kusano, T. Tamano and T. Sato, *Simulation Study of Toroidal Phase-Locking Mechanism in Reversed-Field Pinch Plasma*; Feb. 1991

NIFS-79 K. Nagasaki, K. Itoh and S. -I. Itoh, *Model of Divertor Biasing and Control of Scrape-off Layer and Divertor Plasmas*; Feb. 1991

NIFS-80 K. Nagasaki and K. Itoh, *Decay Process of a Magnetic Island by Forced Reconnection*; Mar. 1991

NIFS-81 K. Takahata, N. Yanagi, T. Mito, J. Yamamoto, O.Motojima and LHDDesign Group, K. Nakamoto, S. Mizukami, K. Kitamura, Y. Wachi, H. Shinohara, K. Yamamoto, M. Shibui, T. Uchida and K. Nakayama, *Design and Fabrication of Forced-Flow Coils as R&D Program for Large Helical Device*; Mar. 1991

NIFS-82 T. Aoki and T. Yabe, *Multi-dimensional Cubic Interpolation for ICF Hydrodynamics Simulation*; Apr. 1991

NIFS-83 K. Ida, S.-I. Itoh, K. Itoh, S. Hidekuma, Y. Miura, H. Kawashima, M. Mori, T. Matsuda, N. Suzuki, H. Tamai, T.Yamauchi and JFT-2M Group, *Density Peaking in the JFT-2M Tokamak Plasma with Counter Neutral Beam Injection* ; May 1991

NIFS-84 A. Iiyoshi, *Development of the Stellarator/Heliotron Research*; May 1991

NIFS-85 Y. Okabe, M. Sasao, H. Yamaoka, M. Wada and J. Fujita, *Dependence of Au^- Production upon the Target Work Function in a Plasma-Sputter-Type Negative Ion Source;* May 1991

NIFS-86 N. Nakajima and M. Okamoto, *Geometrical Effects of the Magnetic Field on the Neoclassical Flow, Current and Rotation in General Toroidal Systems*; May 1991

NIFS-87 S. -I. Itoh, K. Itoh, A. Fukuyama, Y. Miura and JFT-2M Group, *ELMy-H mode as Limit Cycle and Chaotic Oscillations in Tokamak Plasmas;* May 1991

NIFS-88 N.Matsunami and K.Kitoh, *High Resolution Spectroscopy of H^+ Energy Loss in Thin Carbon Film;* May 1991

NIFS-89 H. Sugama, N. Nakajima and M.Wakatani, *Nonlinear Behavior of Multiple-Helicity Resistive Interchange Modes near Marginally Stable States;* May 1991

NIFS-90 H. Hojo and T.Hatori, *Radial Transport Induced by Rotating RF Fields and Breakdown of Intrinsic Ambipolarity in a Magnetic Mirror*; May 1991

NIFS-91 M. Tanaka, S. Murakami, H. Takamaru and T.Sato, *Macroscale Implicit, Electromagnetic Particle Simulation of Inhomogeneous and Magnetized Plasmas in Multi-Dimensions;* May 1991

NIFS-92 S. - I. Itoh, *H-mode Physics, -Experimental Observations and Model Theories-, Lecture Notes, Spring College on Plasma Physics, May 27 - June 21 1991 at International Centre for Theoretical Physics (IAEA UNESCO) Trieste, Italy ;* Jun. 1991

NIFS-93 Y. Miura, K. Itoh, S. - I. Itoh, T. Takizuka, H. Tamai, T. Matsuda, N. Suzuki, M. Mori, H. Maeda and O. Kardaun, *Geometric Dependence of the Scaling Law on the Energy Confinement Time in H-mode Discharges;* Jun. 1991

NIFS-94 H. Sanuki, K. Itoh, K. Ida and S. - I. Itoh, *On Radial Electric Field Structure in CHS Torsatron / Heliotron;* Jun. 1991

NIFS-95 K. Itoh, H. Sanuki and S. - I. Itoh, *Influence of Fast Ion Loss on Radial Electric Field in Wendelstein VII-A Stellarator;* Jun. 1991

NIFS-96 S. - I. Itoh, K. Itoh, A. Fukuyama, *ELMy-H mode as Limit Cycle and Chaotic Oscillations in Tokamak Plasmas;* Jun. 1991

NIFS-97 K. Itoh, S. - I. Itoh, H. Sanuki, A. Fukuyama, *An H-mode-Like Bifurcation in Core Plasma of Stellarators;* Jun. 1991

NIFS-98 H. Hojo, T. Watanabe, M. Inutake, M. Ichimura and S. Miyoshi, *Axial Pressure Profile Effects on Flute Interchange Stability in the Tandem Mirror GAMMA 10;* Jun. 1991

NIFS-99 A. Usadi, A. Kageyama, K. Watanabe and T. Sato, *A Global Simulation of the Magnetosphere with a Long Tail : Southward and Northward IMF;* Jun. 1991

NIFS-100 H. Hojo, T. Ogawa and M. Kono, *Fluid Description of Ponderomotive Force Compatible with the Kinetic One in a Warm Plasma* ; July 1991

NIFS-101 H. Momota, A. Ishida, Y. Kohzaki, G. H. Miley, S. Ohi, M. Ohnishi K. Yoshikawa, K. Sato, L. C. Steinhauer, Y. Tomita and M. Tuszewski *Conceptual Design of D-^{3}He FRC Reactor "ARTEMIS"* ; July 1991

NIFS-102 N. Nakajima and M. Okamoto, *Rotations of Bulk Ions and Impurities in Non-Axisymmetric Toroidal Systems* ; July 1991

NIFS-103 A. J. Lichtenberg, K. Itoh, S. - I. Itoh and A. Fukuyama, *The Role of Stochasticity in Sawtooth Oscillation* ; Aug. 1991

NIFS-104 K. Yamazaki and T. Amano, *Plasma Transport Simulation Modeling for Helical Confinement Systems;* Aug. 1991

NIFS-105 T. Sato, T. Hayashi, K. Watanabe, R. Horiuchi, M. Tanaka, N. Sawairi and K. Kusano, *Role of Compressibility on Driven Magnetic Reconnection ;* Aug. 1991

NIFS-106 Qian Wen - Jia, Duan Yun - Bo, Wang Rong - Long and H. Narumi, *Electron Impact Excitation of Positive Ions - Partial Wave Approach in Coulomb - Eikonal Approximation* ; Sep. 1991

NIFS-107 S. Murakami and T. Sato, *Macroscale Particle Simulation of Externally Driven Magnetic Reconnection;* Sep. 1991

NIFS-108 Y. Ogawa, T. Amano, N. Nakajima, Y. Ohyabu, K. Yamazaki, S. P. Hirshman, W. I. van Rij and K. C. Shaing, *Neoclassical Transport Analysis in the Banana Regime on Large Helical Device (LHD) with the DKES Code;* Sep. 1991

NIFS-109 Y. Kondoh, *Thought Analysis on Relaxation and General Principle to Find Relaxed State;* Sep. 1991

NIFS-110 H. Yamada, K. Ida, H. Iguchi, K. Hanatani, S. Morita, O. Kaneko, H. C. Howe, S. P. Hirshman, D. K. Lee, H. Arimoto, M. Hosokawa, H. Idei, S. Kubo, K. Matsuoka, K. Nishimura, S. Okamura, Y. Takeiri, Y. Takita and C. Takahashi, *Shafranov Shift in Low-Aspect-Ratio Heliotron / Torsatron CHS* ; Sep 1991

NIFS-111 R. Horiuchi, M. Uchida and T. Sato, *Simulation Study of Stepwise Relaxation in a Spheromak Plasma ;* Oct. 1991

NIFS-112 M. Sasao, Y. Okabe, A. Fujisawa, H. Iguchi, J. Fujita, H. Yamaoka and M. Wada, *Development of Negative Heavy Ion Sources for Plasma Potential Measurement* ; Oct. 1991

NIFS-113 S. Kawata and H. Nakashima, *Tritium Content of a DT Pellet in Inertial Confinement Fusion* ; Oct. 1991

NIFS-114 M. Okamoto, N. Nakajima and H. Sugama, *Plasma Parameter Estimations for the Large Helical Device Based on the Gyro-Reduced Bohm Scaling* ; Oct. 1991

NIFS-115 Y. Okabe, *Study of Au^- Production in a Plasma-Sputter Type Negative Ion Source* ; Oct. 1991

NIFS-116 M. Sakamoto, K. N. Sato, Y. Ogawa, K. Kawahata, S. Hirokura, S. Okajima, K. Adati, Y. Hamada, S. Hidekuma, K. Ida, Y. Kawasumi, M. Kojima, K. Masai, S. Morita, H. Takahashi, Y. Taniguchi, K. Toi and T. Tsuzuki, *Fast Cooling Phenomena with Ice Pellet Injection in the JIPP T-IIU Tokamak;* Oct. 1991

NIFS-117 K. Itoh, H. Sanuki and S. -I. Itoh, *Fast Ion Loss and Radial Electric Field in Wendelstein VII-Λ Stellarator*; Oct. 1991

NIFS-118 Y. Kondoh and Y. Hosaka, *Kernel Optimum Nearly-analytical Discretization (KOND) Method Applied to Parabolic Equations <<KOND-P Scheme>>;* Nov. 1991

NIFS-119 T. Yabe and T. Ishikawa, *Two- and Three-Dimensional Simulation Code for Radiation-Hydrodynamics in ICF*; Nov. 1991